The background temperature of the protoplanetary disk within the first four million years of the Solar System

Devin L. Schrader[1]*, Roger R. Fu[2], Steven J. Desch[3], and Jemma Davidson[1]

[1]Center for Meteorite Studies, School of Earth and Space Exploration, Arizona State University, 781 East Terrace Road, Tempe, AZ 85287.

[2]Department of Earth and Planetary Sciences, Harvard University, 20 Oxford St. Cambridge, MA 02138.

[3]School of Earth and Space Exploration, Arizona State University, PO Box 871404, Tempe, AZ 85287.

*Correspondence to: Center for Meteorite Studies, School of Earth and Space Exploration, Arizona State University, Tempe, AZ 85287, (devin.schrader@asu.edu).

Earth and Planetary Science Letters

Volume 504, 15 December 2018, Pages 30–37

Reference:

Schrader D. L., Fu R. R., Desch S. J., and Davidson J. (2018) The background temperature of the protoplanetary disk within the first four million years of the Solar System. *Earth Planet. Sci. Lett.* **504**, 30–37.

https://doi.org/10.1016/j.epsl.2018.09.030

ABSTRACT

The background temperature of the protoplanetary disk is a fundamental but poorly constrained parameter that strongly influences a wide range of conditions and processes in the early Solar System, including the widespread process(es) by which chondrules originate. Chondrules, mm-scale objects composed primarily of silicate minerals, were formed in the protoplanetary disk almost entirely during the first four million years of Solar System history but their formation mechanism(s) are poorly understood. Here we present new constraints on the sub-silicate solidus cooling rates of chondrules at <873 K (600˚C) using the compositions of sulfide minerals. We show that chondrule cooling rates remained relatively rapid (~10^0 to 10^1 K/hr) between 873 and 503 K, which implies a protoplanetary disk background temperature of <503 K (230°C) and is consistent with many models of chondrule formation by shocks in the solar nebula, potentially driven by the formation of Jupiter and/or planetary embryos, as the chondrule formation mechanism. This protoplanetary disk background temperature rules out current sheets and resulting short-circuit instabilities as the chondrule formation mechanism. More detailed modeling of chondrule cooling histories in impacts is required to fully evaluate impacts as a chondrule formation model. These results motivate further theoretical work to understand the expected thermal evolution of chondrules at ≤873 K under a variety of chondrule formation scenarios.

1. INTRODUCTION

Determining the formation mechanism(s) of chondrules and conditions within the protoplanetary disk at this time are key unresolved issues in planetary science with broad implications for the dynamical state and chemical composition of accretion disks and the accretion history of rocky bodies (e.g., Desch et al., 2012). Chondrules, a major component of chondritic meteorites, are partially to fully melted sub-mm to mm-scale sub-spherical objects composed primarily of olivine, pyroxene, and plagioclase with minor amounts of Fe,Ni metal, sulfide, and oxide. Chondrule precursors were flash-heated to peak temperatures for durations on the order of seconds to minutes, then cooled and crystallized on the order of hours to days in the protoplanetary disk (e.g., Hewins et al., 2005; Alexander et al., 2008).

Geochronological analyses indicate that chondrules in most known meteorite groups formed between 0 and 4 million years after the time at which the first solids in the Solar System condensed (=t_0; e.g., Kita et al., 2000; Connelly et al., 2012; Kita and Ushikubo, 2012; Nagashima et al., 2014; Bollard et al., 2017; Krot and Nagashima, 2017; Schrader et al., 2017; Budde et al., 2018). In addition, most chondrules within individual meteorite groups typically formed over a relatively narrow timeframe, ~0.2–0.4 Myr (Kita and Ushikubo, 2012). The chondrule formation process is an active area of debate (e.g., Desch et al., 2012), with current research focusing on heating of precursors in bow shocks around planetary embryos (e.g., Morris et al., 2012; Boley et al. 2013; Mann et al., 2016), large-scale nebular shocks driven by gravitational instabilities (e.g., Desch and Connolly, 2002; Boss and Durisen, 2005; Morris and Desch, 2010; Morris et al., 2016) or in current sheets (e.g., Hubbard et al., 2012; McNally et al.,

2013), or on production of melt droplets by impacts between planetesimals (e.g., Sanders and Scott, 2012; Johnson et al., 2015).

Understanding the complete thermal histories of chondrules is essential to determining their formation mechanism(s) and the conditions of the protoplanetary disk during chondrule formation. Chondrule cooling rates, which are typically constrained based on silicate compositions, textures, and crystallization experiments, range from >5000 K/hr while above the silicate liquidus (>~2023 K) (Yu and Hewins, 1998; Desch and Connolly, 2002), to 5–3000 K/hr while between the silicate liquidus and solidus (~2023–1673 K) (Radomsky and Hewins, 1990; Desch and Connolly, 2002; Hewins et al., 2005; Berlin et al., 2011; Desch et al., 2012; Perez et al., 2018). However, recent crystallization experiments indicate that most chondrules cooled at rates between 300 and 1000 K/hr between the silicate liquidus and solidus (Perez et al., 2018), a narrower range than typically considered. These cooling rates imply that chondrules were in contact with a thermal reservoir during cooling, as isolated chondrules in a vacuum would have cooled from ~2000 to 273 K in a few seconds (Desch et al., 2012; Mann et al., 2016). Therefore, these cooling rates provide information about the physical environment of chondrule formation and have been used to test the validity of chondrule formation models (e.g., Desch et al., 2012).

The vast majority of chondrule cooling rates apply to stages where the chondrule temperature was above the silicate solidus (>1673 K). As such, chondrule cooling rates below the silicate solidus are not as well constrained, despite some previous studies. Cooling rates of ~0.1–60 K/hr during cooling between ~1673–1173 K have been determined using exsolution lamellae in clinopyroxene (Weinbruch et al., 2001). Meanwhile, by studying Cu and Ga diffusive profiles of Fe,Ni metal in Renazzo-like carbonaceous (CR) chondrite chondrules, Humayun (2012) and Chaumard et al. (2018) computed cooling rates of ~0.5–50 K/hr and ~1–90 K/hr, respectively,

during cooling between ~1673–1573 K. Finally, to reproduce plagioclase observed in some chondrules, Wick and Jones (2012) estimated a cooling rate of ~1–25 K/hr between 1273–1073 K.

High-temperature sulfides (i.e., not formed during low-temperature aqueous alteration) provide a potential indicator of cooling rates below their crystallization temperature of ~1261 to ~1223 K, which correspond to the Fe–FeS eutectic and Fe,Ni–FeS eutectic, respectively (Tachibana and Huss, 2005; Tachibana et al., 2006; Schrader et al., 2015, 2016). Comparison of metal-troilite grain textures in LL chondrites with experimental products indicates minimum chondrule cooling rates of 100 K/hr at ~1273 K and much higher maximum rates for grains with a eutectic texture (Tachibana et al., 2006, Mori et al., 2016). Experimental analogs to metal-sulfide grains within CR chondrites suggest maximum cooling rates on the order of 3000 K/hr are possible at ~1273 K (Schrader and Lauretta, 2010). The spread in these cooling rates represents the range of thermal histories recorded by individual chondrules instead of analytical uncertainty. These sulfide-based cooling rates are similar to those determined above the silicate solidus and indicate that chondrules had not begun to approach thermal equilibrium upon cooling to ~1273 K. In contrast, the cooling rates of chondrules below ~1073 K (Wick and Jones, 2012) remain unconstrained. Constraining chondrule cooling rates below 1073 K is crucial to understanding both the background temperature of the protoplanetary disk in which chondrules cooled as well as to test chondrule formation models rigorously to determine the physical processes active in the early Solar System.

Some chondrules in the LL and CR chondrites contain the sulfides pyrrhotite ($[Fe,Ni,Co,Cr]_{1-x}S$) and pentlandite ($[Fe,Ni,Co,Cr]_{9-x}S_8$) in complex intergrowths. These pyrrhotite-pentlandite intergrowths can form by cooling of a primary high-temperature Fe-Ni-S melt, with pentlandite

starting to exsolve during cooling at ~883 K (610°C; e.g., Durazzo and Taylor, 1982; Etschmann et al., 2004). The textures and petrographic setting of these sulfides (i.e., spherical within chondrule mesostases or partially enveloping silicate grains) indicate they were present with the chondrule precursors, became immiscible melts during chondrule heating, and crystallized after silicate minerals (Tachibana et al., 2006; Schrader et al., 2015, 2016). The pyrrhotite-pentlandite intergrowths studied here were previously determined, based on their texture and sulfide geothermometry using experimentally determined Fe-Ni-S phase diagrams (e.g., Raghavan, 2004), to have equilibrated during chondrule cooling below 873 K (Schrader et al., 2015, 2016). Therefore, the sulfides studied here are primary sulfides that formed prior to accretion of their host chondrules into asteroids (e.g., Schrader et al., 2015, 2016; Singerling and Brearley, 2018). Using laboratory cooling experiments of Ni-rich Fe-Ni-S charges, Etschmann et al. (2004) determined that the bulk composition of the sulfide and abundance of pentlandite exsolved are related to the cooling rate. These cooling experiments utilized four different starting compositions for the charges (from $Fe_{0.9}Ni_{0.1}S$, $Fe_{0.85}Ni_{0.15}S$, $Fe_{0.8}Ni_{0.2}S$, and $Fe_{0.7}Ni_{0.3}S$), and were cooled from 973 to 373 K over 24 hrs but were observed at different time steps. The exsolution reaction rate constants and parameters were determined for each bulk composition studied. Initial pentlandite exsolution was rapid, commencing at ~873 K and ceasing at ~548 K (Etschmann et al., 2004). Depending on the bulk composition and the cooling time, the sulfides contained different abundances of pentlandite (Etschmann et al., 2004). The morphology of pentlandite-pyrrhotite intergrowths are related to cooling rate, with quenching found to result in randomly oriented blebs of pentlandite in pyrrhotite (Francis et al., 1976), while slow cooling (~1 to 60 K/hr) results in oriented pentlandite lamellae in pyrrhotite (Francis et al., 1976; Durazzo and Taylor, 1982; Etschmann et al., 2004). We studied the morphology and

composition of sulfides in CR and LL chondrites and compared them to sulfide laboratory experiments to (1) determine the sub-silicate solidus chondrule cooling rates, (2) constrain the background temperature of the protoplanetary disk, and (3) test chondrule formation models.

2. MATERIALS AND METHODS

2.1. Calculating sub-silicate solidus cooling rates

We studied sulfide-bearing opaque assemblages in type II (FeO-rich, Fe/(Fe + Mg) > 10% atomic ratio) chondrules from ten CR2 chondrites: Elephant Moraine (EET) 87770,31, EET 92048,7, Gao-Guenie (b) UA2301,1, Graves Nunataks 95229,22, LaPaz Icefield **(**LAP) 02342,14, LAP 04720,8, Miller Range (MIL) 090657,6, Pecora Escarpment (PCA) 91082,15, Queen Alexandra Range 99177,6, and Yamato 793495,72-2. We also examined type I (FeO-poor, Fe/(Fe + Mg) < 10% atomic ratio) and type II chondrules from the LL3.00 chondrite Semarkona USNM1805-17.

We characterized thin sections via optical microscopy, an FEI Nova NanoSEM 600 scanning electron microscope and JEOL 8900 Superprobe electron probe microanalyzer (EPMA) at the Smithsonian Institution National Museum of Natural History, Department of Mineral Sciences, a Cameca SX-50 and an SX-100 EPMA at the University of Arizona, and a JEOL JXA-8530F EPMA at Arizona State University (Electronic Annex [EA]-1). Standards and detection limits for the EPMA analyses are given in EA-2. Sulfide bulk compositions were determined by modal recombination analysis using analyses of individual mineral phases via EPMA combined with

modal mineralogy (obtained in Adobe Photoshop®) and phase densities (e.g., Berlin et al., 2011; Schrader et al., 2015).

We compiled the bulk compositions of 51 sulfide-bearing opaque assemblages from 20 chondrules. Among these, the compositions of 44 assemblages from 15 CR chondrite chondrules were taken from Schrader et al. (2015). The sulfides studied were typically smaller than 0.1 mm in diameter (EA-1), similar to the grain sizes of sulfides used in comparable experimental studies (Francis et al., 1976; Durazzo and Taylor, 1982; Etschmann et al., 2004). In addition, we analyzed the bulk compositions of one sulfide-bearing opaque assemblage from a chondrule in EET 92048 (CR2) and two sulfide-bearing opaque assemblages from a chondrule in MIL 090657 (CR2). Finally, we include four compositions of sulfide-bearing opaque assemblages from three chondrules from the LL3.00 chondrite Semarkona (*in situ* analyses from Schrader et al. [2016] and this study; EA-2). Of these 51 sulfide-bearing opaque assemblages, only 28 have both pyrrhotite and pentlandite, making them candidates for calculating cooling rates (e.g., Fig. 1 and EA-1). Of these 28, only eight have metal (Fe and Ni) to sulfur ratios (M:S) compatible with the sulfides used in experiments of Etschmann et al. (2004) (M:S ~1) and $y \leq 1$, where y is the fraction of material transformed (i.e., the degree of pentlandite exsolution; Etschmann et al., 2004). The eight sulfides with M:S ~ 1 and $y \leq 1$ only consist of pyrrhotite and pentlandite, the same as that in the experimental products of (Etschmann et al., 2004). The morphologies of these sulfides are oriented lamellae and/or blocky pentlandite within pyrrhotite (EA-1), indicating relatively slow cooling (e.g., Francis et al., 1976; Durazzo and Taylor, 1982; Etschmann et al., 2004).

We computed cooling rates by utilizing compositional data obtained from sulfides in chondrules (see above) and applying the appropriate reaction rate constants for pentlandite

exsolution in different bulk compositions as determined by Etschmann et al. (2004). These constants were applied to natural sulfides by using the Avrami equation, which can be written as (Etschmann et al., 2004):

$$y = 1 - \exp(-k^n t^n) \text{ (Eq. 1).}$$

Where k is the rate constant (in 1/s), t is time (in s), n is the Avrami geometric constant (dependent on the reaction/growth mechanism for pentlandite), and y is the fraction of material transformed (Etschmann et al., 2004). We then obtain an expression for the cooling timescale:

$$t = k^{-1} \left(\ln [1-y]^{-1} \right)^{1/n} \text{ (Eq. 2)}$$

Etschmann et al. (2004) determined their k values at the beginning of the exsolution reaction, which represents the most rapid stage of the process. The value of y varies between 0 and 1 and is determined by ascertaining how far towards completion the exsolution reaction has progressed (Table 1). Etschmann et al. (2004) determined for each studied bulk composition that $y = 1$ when the remaining pyrrhotite contained no Ni, meaning that all Ni had partitioned into the exsolved pentlandite. The wt.% pentlandite for each bulk composition where $y = 1$ was determined by Etschmann et al. (2004).

The Avrami equation (Eq. 1) is an isothermal equation; however, Etschmann et al. (2004) found that the n and some of the k values for pentlandite exsolution vary only slightly with temperature between 873 and 548 K. To apply these reaction rates to natural sulfides, we used the temperature ranges of exsolution determined from sulfide geothermometry. Sulfides in the

CR chondrite chondrules equilibrated between 873 and 673 K (Schrader et al., 2015), a temperature range of 200 K. Meanwhile, sulfides in the LL3.00 chondrite Semarkona equilibrated between 873 and 503 K (Schrader et al., 2016), a wider range of 370 K. We used the mean n value for each bulk composition, and the mean k value when necessary (only for the $Fe_{0.9}Ni_{0.1}S$ case; Etschmann et al., 2004) between 873 and 673 K for CR chondrite sulfides, and between 873 and 503 K for the LL3.00 chondrite sulfides. The oriented morphology of pentlandite in pyrrhotite indicates the sulfides cooled slowly during their formation (e.g., Francis et al., 1976). However, since we cannot rule out that the cooling rates changed during cooling, we note that these cooling rates are average cooling rates over the temperature range investigated.

To verify that we did not bias the data outside of typical uncertainties by using the single k value and mean n values, we recalculated each cooling rate by using the full range of n and k values in each experiment of Etschmann et al. (2004). We found that the cooling rates only decrease by a maximum of ~3.8 K/hr (for Gao-Guenie (b) Ch12 Al; Table 1), with a decrease of <1 K/hr for all other cases. These values fall well within uncertainties discussed below. Since k values were determined during the most rapid stage of exsolution (Etschmann et al., 2004) and k may decrease during cooling, actual cooling timescales for the chondrule sulfides may be longer and their cooling rates would be lower than calculated. However, the morphological similarity between chondrule sulfides and experimental sulfides indicates they cooled at similar rates (e.g., ~1–60 K/hr; Francis et al., 1976; Durazzo and Taylor, 1982; Etschmann et al., 2004). Therefore, these assumptions about the temperature range of exsolution permit us to constrain accurately the approximate cooling rate of chondrules between 873 and 503 K.

To determine the value of y for each natural sulfide (Table 1), we took the ratio of the amount of exsolved pentlandite in wt.% in the natural sulfides to the amount determined by Etschmann et al. (2004) of the complete exsolution reaction for each bulk composition. We could proceed with determining the cooling rate if $y < 1$ (the exsolution reaction was incomplete). No natural sulfides were found with $y = 1$ (i.e., complete exsolution of pentlandite with no Ni remaining in pyrrhotite) indicating that the chondrule sulfides cooled before the exsolution reactions were complete. If the bulk composition of the sulfide was out of the range of the Etschmann et al. (2004) experiments, or if $y > 1$, then we could not determine a rate for that sulfide. In cases of $y > 1$, it is possible that due to thin sectioning resulting in a 2D slice of a 3D object, we obtained a biased sample of that particular sulfide grain (i.e., we observed more pentlandite than the bulk sulfide actually contained). However, considering that the cooling rates determined for all sulfides (Table 1) are similar to one another, we argue that the cooling rates determined here are representative.

To determine the cooling rates, if the bulk composition of the natural sulfide was within ~5 at.% of the experimental bulk compositions (Etschmann et al., 2004), we applied the n and k values of the closest bulk composition and used Equation 2 to solve for the cooling time (t in seconds). To determine the cooling rate, the temperature range determined for pentlandite exsolution, $\Delta T = 200$ K for the CR chondrite sulfides, and $\Delta T = 370$ K for the LL3.00 chondrite sulfides, was divided by the cooling time (in hours);

$$\Delta T / t(\text{hr}) = \text{cooling rate (Eq. 3)}.$$

We did not use bulk compositions of sulfides that differed from those of experiments by more than 5 at.% Ni.

Most sulfides studied here had a higher bulk Ni content, more exsolved pentlandite, or higher M:S ratios than the experimental charges. Thus, we were only able to constrain cooling rates for 6 out of 24 pyrrhotite and pentlandite-bearing sulfides from CR chondrites (this study; Schrader et al., 2015) and two out of four from the LL3.00 chondrite (this study; Schrader et al., 2016) from a total of seven different chondrules (Table 1). Since the sulfides with higher bulk Ni content exsolve pentlandite faster than sulfides with less bulk Ni (Etschmann et al., 2004), we suggest the remaining sulfides cooled on similar or at faster rates than those constrained here (Table 1).

2.2. Estimating uncertainties on cooling rates

To determine the maximum variation in the calculated cooling rates, and therefore the uncertainty in the rates, each cooling rate was re-calculated using the values (i.e., k, n, and recalculating the y value) of the experimental charge with next nearest bulk composition (i.e., a maximum of 10 at.% Ni different than the bulk composition of the sulfide). For example, if the bulk composition of the sulfide was 5 at.% Ni, we used the values for the 10 at.% Ni case to determine the cooling rate, and the 15 at.% case to determine the maximum uncertainty. As an example, by applying the $Fe_{0.85}Ni_{0.15}S$ values to a natural sulfide closest to the $Fe_{0.9}Ni_{0.1}S$ case, the cooling rate changes from 0.3 K/hr to 15 K/hr (for Gao-Guenie (b) Ch1 A5). For the sulfide with the fastest calculated cooling rate (Gao-Guenie (b) Ch12 A1), the natural sulfide has 5 at.% Ni, and we therefore used the $Fe_{0.9}Ni_{0.1}S$ case, and obtained a cooling rate of 4.3 K/hr (Table 1).

If we instead had used the constants from the next closest bulk composition of $Fe_{0.85}Ni_{0.15}S$, we would have obtained a cooling rate of 51 K/hr. Therefore, we estimate our maximum uncertainties are ~45 K/hr, or one order of magnitude. However, these are extreme cases (using at.% Ni cases beyond 5 at.% Ni), and we argue that our typical uncertainties are lower for the cases where the bulk compositions were closest to the experimental charges used. A minimum uncertainty of ~2 K/hr can be estimated from the only case where cooling rates were determined for two sulfides in a single chondrule (Table 1; Semarkona Ch3; 0.3 K/hr and 2 K/hr). Therefore, we estimate the uncertainties in our cooling rates are typically within ~2 K/hr, and are at most within an order of magnitude (i.e., ~45 K/hr).

3. RESULTS

By comparing the morphologies and compositions of natural pyrrhotite-pentlandite assemblages (Fig. 1 and EA-1) to chemical reaction rates determined for pentlandite exsolution during cooling (Etschmann et al., 2004) and the textures of laboratory made sulfides (Francis et al., 1976; Durazzo and Taylor, 1982), we calculated cooling rates for chondrule sulfide assemblages. We determined approximate cooling rates by calculating the exsolution timescale for each sulfide assemblage over the equilibration temperature range of 200 K for the CR chondrite sulfides (Schrader et al., 2015) and 370 K for LL3.00 chondrite sulfides (Schrader et al., 2016). These estimated cooling rates are between ~0.3 and ~4 K/hr (mean ~1 K/hr) for the CR chondrites and between 0.3 and 2 K/hr (mean ~1 K/hr) for the LL3.00 chondrite (Table 1). For comparison, experimental analogs to terrestrial Ni-sulfide ores with similar textures as the chondrule sulfide assemblages studied here (EA-1; oriented lamellae and blocky pentlandite in

pyrrhotite) were cooled in the laboratory at 1 K/hr (Durazzo and Taylor, 1982), which is remarkably close to our values. The *in situ* cooling experiments of Etschmann et al. (2004) were cooled at 10 K/hr, and Etschmann et al. (2004) noted similar textures to those of Durazzo and Taylor (1982). Assuming chondrules in each meteorite group cooled uniformly, the range in cooling rates for the sulfides indicate minimum uncertainties of ~±3 K/hr. Meanwhile, more conservative analysis of uncertainties shows that they are at most within an order of magnitude (see Section 2.2). Therefore, we conclude that, between 873 and 673 K for the CR chondrites, and 873 and 503 K for the LL3.00 chondrite, chondrules cooled at rates of ~10^0 to 10^1 K/hr (Fig. 2). These cooling rates imply that CR chondrules cooled between 873 and 673 K in ~20 to 200 hrs, and LL3.00 chondrite chondrules cooled between 873 and 503 K in ~37 to 370 hrs.

4. DISCUSSION

In this study we determined approximate average chondrule cooling rates at temperatures below 873 K to constrain the protoplanetary disk background temperature between ~1 to 4 million years after the first solids formed in the Solar System. We accomplished this by studying sulfide assemblages in chondrules from chondrites that remain nearly unaltered since their accretion and applying chemical reaction rates determined from sulfides prepared in the laboratory. These cooling rates are then used to test models of chondrule formation. To cover a range of chondrule-forming environments, we studied chondrules from the LL and CR chondrite groups, which formed between ~1 to 3 Ma (Kita et al., 2000; Kita and Ushikubo, 2012) and ~2 to 4 Ma (mean ~$3.7^{+0.3}_{-0.2}$ Ma; Schrader et al., 2017) after $t_{0,}$ respectively (Nagashima et al., 2014; Schrader et al., 2017; Budde et al., 2018), assuming ^{26}Al was homogeneously distributed in the

protoplanetary disk (e.g., Kita and Ushikubo, 2012; Schrader et al., 2017; Budde et al., 2018). In addition to forming earlier, several lines of evidence suggest that LL chondrite chondrules formed closer to the Sun than those from CR chondrites, with the LL chondrites likely forming in the inner Solar System and the CR chondrites forming outside the orbit of an early Jupiter (e.g., Ghosh et al., 2006; Kruijer et al., 2016; Van Kooten et al., 2016; Desch et al., 2018; Schrader et al., 2018).

Chondrule formation occurred in differing windows of short timescales (i.e., typically within ~0.2–0.4 Myr) for chondrules within individual meteorite groups (Kita and Ushikubo, 2012). Some chondrules record evidence for multiple flash heating events. However, whether or not the chondrules studied here experienced multiple heating events, our estimated sulfide cooling rates constrain the sub-silicate solidus cooling rates of chondrule formation. Evidence for reheating event(s) after initial silicate crystallization includes the presence of relict grains, enveloped chondrules, and igneous rims (e.g., Jones, 1996; Rubin and Krot, 1996). The presence of volatile elements in chondrules restricts the duration of these heating events to be on the order of seconds to minutes, commonly referred to as flash heating (e.g., Hewins et al., 2005; Alexander et al., 2008). Nebular reheating events could only alter chondrule sulfides if the peak temperatures were higher than the liquidus temperature of these sulfides (~1261 to ~1223 K), as lower temperature modification requires sustained temperatures of days to years (experimentally shown by Etschmann et al. [2004] and Durazzo and Taylor [1982]). If the sulfides studied here had been altered in a secondary heating event(s), such events were part of chondrule formation and the sulfide cooling rates still record the sub-silicate solidus cooling rates of chondrules.

4.1. Background temperature of the protoplanetary disk

Chondrule cooling rates should slow down significantly as they approach the background temperature of the protoplanetary disk. Average chondrule cooling rates between the silicate liquidus and solidus (~2023–1673 K) are 10^1 to 10^3 K/hr and 10^0 to 10^3 K/hr between 1673–1073 K (see Introduction). Therefore, the chondrule cooling rates of ~10^0 to 10^1 K/hr between 873 and 503 K have slowed compared to cooling rates above 1073 K but have not ceased altogether, indicating that the background temperature of the protoplanetary disk was <503 K. Chondrule textures are related to peak melting temperature, with barred olivine chondrules being heated to higher temperatures than porphyritic chondrules (e.g., Hewins et al., 2005) and agglomeratic olivine chondrules experiencing the lowest peak temperature of <1473 K (e.g., Weisberg and Prinz, 1996; Schrader et al., 2018). There is no relationship between sub-silicate solidus cooling rates and chondrule textural or chemical type (Table 1 and Fig. 1), indicating peak heating temperature and oxygen fugacity during chondrule formation do not influence sub-silicate solidus cooling rates. Since we observe consistent cooling rates for chondrules that formed between ~1 and ~4 Ma after t_0 (Kita et al., 2000; Kita and Ushikubo, 2012; Nagashima et al., 2014; Schrader et al., 2017) and likely at a range of heliocentric distances (e.g., Ghosh et al., 2006; Kruijer et al., 2016; Van Kooten et al., 2016; Desch et al., 2018), we conclude that the protoplanetary disk background temperature was <503 K in all the times and places in the solar nebula where CR and LL chondrite chondrules formed.

Previously, the best estimate on the background temperature of the protoplanetary disk was <650 K (the 50% condensation temperature of S; Rubin et al., 1999), which was based on the presence of primary sulfides (pre-accretionary, not formed on the parent asteroid; e.g., Rubin et al., 1999; Tachibana and Huss, 2005; Schrader et al., 2015, 2016) in chondrules. Our results

indicate that the protoplanetary disk background temperature was much lower than this, at <503 K. This is consistent with protoplanetary disk models, which generally predict temperatures <503 K in the inner disk (e.g., Boss, 1998; Min et al., 2011).

4.2. Testing chondrule formation models

These sub-silicate solidus cooling rates also provide an experimental constraint on chondrule formation models. One proposed model of chondrule formation is heating via current sheets and resulting short-circuit instabilities (Hubbard et al., 2012; McNally et al., 2013). A requirement of this model is that the background temperature of the protoplanetary disk must have been high enough to facilitate thermal ionization, implying a minimum of 800 K (McNally et al., 2013; Desch and Turner, 2015). If an initial background temperature of 850 K is considered, short-circuit instability models lead to peak temperatures of 1600 K, high enough to melt precursor chondrule silicates (McNally et al., 2013). Since the background temperature of the protoplanetary disk during chondrule formation was below 503 K, we find that the conditions did not exist to facilitate heating via current sheets and resulting short-circuit instabilities.

Cooling rate estimates for chondrules formed in impacts of <60 K/hr (Johnson et al., 2015) might be consistent with sub-silicate solidus chondrule cooling rates determined here. However, this model did not make predictions for cooling rates at different temperatures and therefore more detailed modeling of cooling rates from impacts will be required to fully evaluate this chondrule formation model.

Chondrules proposed to form via eccentric planetary embryo bow shocks, which may have been triggered by the formation of Jupiter gravitationally interacting with pre-existing

embryos, have a range of cooling rates that depend on embryo size (Mann et al., 2016). Some of the slowest cooling rates, which assume a background temperature for the protoplanetary disk of ~300 K (Mann et al., 2016), are similar to those determined here, particularly those with no radiation (adiabatic) or radiation with low opacity. Cooling rates between temperatures of 873 and 503 K predicted from bow shocks are typically on the order of 10^2 K/hr (e.g., Mann et al., 2016), at least an order of magnitude higher than the approximate rates determined here (i.e., 10^0 to 10^1 K/hr; Table 1 and Fig. 2). Since chondrule cooling rates generally decrease with increasing embryo size, and embryos at least as large as Mars would yield slower cooling rates (Mann et al. 2016), the cooling rates determined here are consistent with current models of chondrule formation in bow shocks preceding larger embryos.

Cooling rates modeled for chondrule formation in large-scale shocks, which can be driven by gravitational instabilities in the protoplanetary disk (Boss and Durisen, 2005; Desch et al., 2012; Morris et al., 2016), are on the order of 10^1 K/hr between 1800 and 1600 K (Morris and Desch, 2010; Morris et al., 2016). Calculations that allow escape of radiation to a cold (e.g., ~300 K) background yield cooling rates ~10^1 K/hr at ~503 K (Morris and Desch, 2010), which are consistent with the cooling rates determined here. Modeled disks in which Jupiter forms at ~5.2 AU have strong gravitational instability-driven shocks starting at t_0 that last for several Myr, and material in the disk between ~2 and 3 AU (the suspected formation region of many chondrules) is particularly heated due to the shock front (Boss and Durisen, 2005). The shocks persist before and after the formation of Jupiter, as Jupiter then drives strong shocks in the inner disk, until the gas and dust dissipates (Boss and Durisen, 2005). However, since chondrules from some meteorite groups likely formed outside the orbit of Jupiter (e.g., Kruijer et al., 2016; Van Kooten et al., 2016; Desch et al., 2018; Schrader et al., 2018), further modeling is required to test if

material outside the orbit of Jupiter can be sufficiently heated by this mechanism to form chondrules.

Shocks existing prior to and during the accretion of Jupiter are consistent with chondrule geochronology (1–4 Ma after t_0; e.g., Kita et al., 2000; Kita and Ushikubo, 2012; Nagashima et al., 2014; Schrader et al., 2017; Budde et al., 2018) and the formation timeframe of Jupiter. Chondrule formation by shocks is consistent with the accretion age of Jupiter; Kruijer et al. (2016) places its core formation at <1 Ma with accretion lasting until 3 to 4 Ma after t_0. Therefore, the formation time of Jupiter is fully consistent with its role in propagating gravitational instability shocks and/or eccentric planetary embryo bow shocks leading to the formation of chondrules.

5. CONCLUSIONS

1. Using the compositions of sulfide minerals compared to experimental analogs, we determined the sub-silicate solidus cooling rates of chondrules at <873 K (600˚C) in order to constrain both the background temperature of the protoplanetary disk and provide a new test for models of chondrule formation.
2. We determined that chondrule cooling rates of chondrules that formed at different times and heliocentric distances remained relatively rapid between 873 and 503 K, at ~10^0 to 10^1 K/hr, which implies a background temperature of the protoplanetary disk <503 K (230°C). This background temperature rules out current sheets and resulting short-circuit instabilities as a chondrule formation mechanism.

3. The sub-silicate solidus chondrule cooling rates are consistent with many shock models in the early Solar System as the chondrule formation mechanism, potentially driven by the formation of Jupiter and/or planetary embryos. However, these cooling rates do not indicate a particular shock mechanism or rule out formation of chondrules via impacts. Instead, these results motivate further theoretical work to understand chondrule cooling histories ≤873 K under a variety of chondrule formation scenarios.

REFERENCES

Alexander C. M. O'D., Grossman J. N., Ebel D. S. and Ciesla F. J. (2008) The formation conditions of chondrules and chondrites. *Science* **320**, 1617–1619.

Berlin J., Jones R. H., and Brearley A. J. (2011) Fe–Mn systematics of type IIA chondrules in unequilibrated CO, CR, and ordinary chondrites. *Meteorit. Planet. Sci.* **46**, 513–533.

Boley A. C., Morris M. A., and Desch S. J. (2013) High-temperature processing of solids through solar nebular bow shocks: 3D radiation hydrodynamics simulations with particles. *Astrophys. J.* **776**, 101–123.

Bollard J., Connelly J. N., Whitehouse M. J., Pringle E. A., Bonal L., Jørgensen J. K., Nordlund Å., Moynier F., and Bizzarro M. (2017) Early formation of planetary building blocks inferred from Pb isotopic ages of chondrules. *Sci. Adv.* **3**, e1700407.

Boss A. P. (1998) Temperatures in protoplanetary disks. *Annu. Rev. Earth Planet. Sci.* **26**, 53–80.

Boss A. P. and Durisen R. H. (2005) Chondrule-forming shock fronts in the solar nebula: A possible unified scenario for planet and chondrite formation. *Astrophys. J.* **621**, L137–L140.

Budde G., Kruijer T. S. and Kleine T. (2018) Hf-W chronology of CR chondrites: Implications for the timescales of chondrule formation and the distribution of 26Al in the solar nebula. *Geochim. Cosmochim. Acta* **222**, 284–304.

Chaumard N., Humayun M., Zanda B., and Hewins R. H. (2018) Cooling rates of type I chondrules from Renazzo: Implications for chondrule formation. *Meteorit. Planet. Sci.* **53**, 984–1005.

Connelly J. N., Bizzarro M., Krot A. N., Nordlund A., Wielandt D., and Ivanova M. A. (2012) The absolute chronology and thermal processing of solids in the solar protoplanetary disk. *Science* **338**, 651–655.

Desch S. J. and Connolly H. C. Jr. (2002) A model of the thermal processing of particles in solar nebula shocks: Application to the cooling rates of chondrules. *Meteorit. Planet. Sci.* **37**, 183–207.

Desch S. J. and Turner N. J. (2015) High-temperature ionization in protoplanetary disks. *Astrophys. J.* **811**, 156–172.

Desch S. J., Morris M. A., Connolly H. C. Jr., and Boss A. P. (2012) The importance of experiments: Constraints on chondrule formation models. *Meteorit. Planet. Sci.* **47**, 1139–1156.

Desch S. J., Kalyaan A., and Alexander C. M. O'D. (2018) The effect of Jupiter's formation on the distribution of refractory elements and inclusions in meteorites. *Astrophys. J. (in press),* arXiv:1710.03809v1

Durazzo A. and Taylor L. A. (1982) Exsolution in the mss-pentlandite system: Textural and genetic implications for Ni-sulfide ores. *Mineral. Deposita* **17**, 313-332.

Etschmann B., Pring A., Putnis A., Grguric B. A., and Studer A. (2004) A kinetic study of the exsolution of pentlandite $(Ni,Fe)_9S_8$ from the monosulfide solid solution (Fe,Ni)S. *Am. Mineral.* **89**, 39–50.

Francis C. A., Fleet M. E., Misra K., and Craig J. R. (1976) Orientation of exsolved pentlandite in natural and synthetic nickeliferious pyrrhotite. *Am. Mineral.* **61**, 913–920.

Ghosh A., Weidenschilling S. J., McSween H. Y. Jr., and Rubin A. (2006) "Asteroidal heating and thermal stratification of the asteroid belt" in *Meteorites and the Early Solar System II*, D. S. Lauretta and H. Y. McSween, Eds. (University of Arizona Press, Tucson), pp. 555–566.

Hewins R. H., Connolly H. C. Jr., Lofgren G. E., and Libourel G. (2005) "Experimental constraints on chondrule formation" in Chondrites and the Protoplanetary Disk (Astronomical Society of the Pacific, San Francisco), pp. 286–316.

Hubbard A., McNally C. P., Mac Low M-M. (2012) Short circuits in thermally ionized plasmas: A mechanism for intermittent heating of protoplanetary disks. *Astrophys. J.* **761**, 58–69.

Humayun M. (2012) Chondrule cooling rates inferred from diffusive profiles in metal lumps from theAcfer 097 CR2 chondrite. *Meteorit. Planet. Sci.* **47**, 1191–1208.

Johnson B. C., Minton D. A., Melosh H. J., and Zuber M. T. (2015) Impact getting as the origin of chondrules. *Nature* **517**, 339–341.

Jones R. H. (1996) Relict grains in chondrules: Evidence for chondrule recycling. In *Chondrules and the Protoplanetary Disk* (eds. R. H. Hewins, R. Jones and E. Scott), pp. 163–172.

Kita N. T. and Ushikubo T. (2012) Evolution of protoplanetary disk inferred from ^{26}Al chronology of individual chondrules. *Meteorit. Planet. Sci.* **47**, 1108–1119.

Kita N. T.,Nagahara H., Togashi S., and Morishita Y. (2000) A short duration of chondrule formation in the solar nebula: Evidence from ^{26}Al in Semarkona ferromagnesian chondrules. *Geochim. Cosmochim. Acta* **64**, 3913–3922.

Krot A. N. and Nagashima K. (2017) Constraints on mechanisms of chondrule formation from chondrule precursors and chronology of transient heating events in the protoplanetary disk. *Geochem. J.* **51**, 45–68.

Kruijer T. S., Burkhardt C., Budde G., and Kleine T. (2016) Age of Jupiter inferred from the distinct genetics and formation times of meteorites. *P Natl. Acad. Sci. USA* **114**, 6712-6716.

Mann C. R., Boley A. C., and Morris M. A. (2016) Planetary embryo bow shocks as a mechanism for chondrule formation. *Astrophys. J.* **818**, 103–122.

McNally C. P., Hubbard A., Mac Low M-M., Ebel D. S., and D'Alessio P. (2013) Mineral processing by short circuits in protoplanetary disks. *Astrophys. J. Lett.* **767**, L2.

Min M., Dullemond C. P., Kama M., and Dominik C. (2011) The thermal structure and the location of the snow line in the protosolar nebula: Axisymmetric models with full 3-D radiative transfer. *Icarus* **212**, 416–426.

Mori M., Tachibana S., Piani L., Marrocchi Y., Schrader D. L., and Connolly H. C., Jr. (2016) Cooling experiments of Fe-FeS melt: A cooling speedometer of chondrules. 26th Goldschmit Conference.

Morris M. A., Boley A. C., Desch S. J., and Athanassiadou T. (2012) Chondrule formation in bow shocks around eccentric planetary embryos. *Astrophys. J.* **752**, 27–43.

Morris M. A. and Desch S. J. (2010) A re-evalution of chondrule formation in large-scale shocks. (abstract #2577), 45th Lunar and Planetary Science Conference. CD-ROM.

Morris M. A., Weidenschilling S. J., and Desch S. J. (2016) The effect of multiple particle sizes on cooling rates of chondrules produced in large-scale shocks in the solar nebula. *Meteorit. Planet. Sci.* **51**, 870–883.

Nagashima K., Krot A. N., and Huss G. R. (2014) ^{26}Al in chondrules from CR2 chondrites. *Geochem. J.* **48**, 561–570.

Perez A. M., Desch S. J., Schrader D. L., and Till C. B. (2018) An experimental investigation of the planetary embryo bow shock model as a chondrule formation mechanism. (abstract #2041). 49th Lunar and Planetary Science Conference. CD-ROM.

Radomsky P. M. and Hewins R. H. (1990) Formation conditions of pyroxene-olivine and magnesian olivine chondrules. *Geochim. Cosmochim. Acta* **54**, 3475–3490.

Raghavan V. (2004) Fe–Ni–S (iron–nickel–sulfur). *J. Phase Equilib.* **25**, 373–381.

Rubin A. E. and Krot A. N. (1996) Multiple heating of chondrules. In *Chondrules and the Protoplanetary Disk* (eds. R. H. Hewins, R. Jones and E. Scott), pp. 173–180.

Rubin A. E., Sailer A. L., and Wasson J. T. (1999) Troilite in the chondrules of type-3 ordinary chondrites: Implications for chondrule formation. *Geochim. Cosmochim. Acta* **63**, 2281–2298.

Sanders I. S. and Scott E. R. D. (2012) The origin of chondrules and chondrites: Debris from low-velocity impacts between molten planetesimals? *Meteorit. Planet. Sci.* **47**, 2170-2192.

Schrader D. L. and Lauretta D. S. (2010) High-temperature experimental analogs of primitive meteoritic metal-sulfide-oxide assemblages. *Geochim. Cosmochim. Acta* **74**, 1719–1733.

Schrader D. L., Connolly H. C. Jr., Lauretta D. S., Zega T. J., Davidson J., and Domanik K. J. (2015) The formation and alteration of the Renazzo-like carbonaceous chondrites III: Toward understanding the genesis of ferromagnesian chondrules. *Meteorit. Planet. Sci.* **50**, 15–50.

Schrader D. L., Davidson J., and McCoy T. J. (2016) Widespread evidence for high-temperature formation of pentlandite in chondrites. *Geochim. Cosmochim. Acta*. **189**, 359–376.

Schrader D. L., Nagashima K., Krot A. N., Ogliore R. C., Yin Q.-Z., Amelin Y. A., Stirling C. H., and Kaltenbach A. (2017) Distribution of ^{26}Al in the CR chondrite chondrule-forming region of the protoplanetary disk. *Geochim. Cosmochim. Acta*. **201**, 275–302.

Schrader D. L., Nagashima K., Waitukaitis S. R., Davidson J., McCoy T. J., Connolly Jr. H. C., and Lauretta D. S. (2018) The retention of dust in protoplanetary disks: Evidence from agglomeratic olivine chondrules from the outer Solar System. *Geochim. Cosmochim. Acta.* **223**, 405–421.

Singerling S. A. and Brearley A. J. (2018) Primary iron sulfides in CM and CR carbonaceous chondrites: Insights into nebular processes. *Meteorit. Planet. Sci.* **53**, 2078–2106.

Tachibana S. and Huss G. R. (2005) Sulfur isotope composition of putative primary troilite in chondrules from Bishunpur and Semarkona. *Geochim. Cosmochim. Acta* **69**, 3075–3097.

Tachibana S., Nagahara H., and Mizuno K. (2006) Constraints on cooling rates of chondrules from metal-troilite assemblages. (abstract #2263), 37th Lunar and Planetary Science Conference. CD-ROM.

Van Kooten E. M. M. E. , Wielandt D., Schiller M., Nagashima K., Thomen A., Larsen K. K., Olsen M. B., Norlund A., Krot A. N., and Bizzarro M. (2016) Isotopic evidence for primordial molecular cloud material in metal-rich carbonaceous chondrites. *P Natl. Acad. Sci. USA* **113**, 2011–2016.

Weisberg M. K. and Prinz M. (1996) Agglomeratic chondrules, chondrule precursors, and incomplete melting. In *Chondrules and the Protoplanetary Disk* (eds. R. H. Hewins, R. Jones and E. Scott), pp. 119–128.

Weinbruch S., Müller W. F., and Hewins R. H. (2001) A transmission electron microscope study of exsolution and coarsening in iron-bearing clinopyroxene from synthetic analogues of chondrules. *Meteorit. Planet. Sci.* **36**, 1237–1248.

Wick M. J. and Jones R. H..(2012) Formation conditions of plagioclase-bearing type I chondrules in CO chondrites: A study of natural samples and experimental analogs. *Geochim. Cosmochim. Acta* **98**, 140–159.

Yu Y. and Hewins R. H. (1998) Transient heating and chondrule formation: Evidence from sodium loss in flash heating simulation experiments. *Geochim. Cosmochim. Acta* **62**, 159–172.

Acknowledgments:

For supplying the samples that were necessary for this work, the authors would like to thank: the Smithsonian Institution, the members of the Smithsonian Institution, the Meteorite Working Group, Cecilia Satterwhite and Kevin Righter (NASA, Johnson Space Center), Japan's National Institute of Polar Research, and Michael Farmer. US Antarctic meteorite samples are recovered by the Antarctic Search for Meteorites (ANSMET) program, which has been funded by NSF and NASA, and characterized and curated by the Department of Mineral Sciences of the Smithsonian Institution and Astromaterials Curation Office at NASA Johnson Space Center. The authors thank Ken Domanik and Axel Wittmann for assistance with the electron microprobes at UA and ASU, respectively. We are also grateful to two anonymous reviewers and Editor Frederic Moynier, whose constructive comments improved the quality of the manuscript. This work was funded in part by NASA grant NNX17AE53G (PI: DLS) and the Center for Meteorite Studies, Arizona State University.

TABLES

Table 1. Minimum sulfide cooling rates.

Group	Meteorite	Chondrule	Chondrule Texture	Chondrule Type	Sulfide Assemblage	Equilibraiton Temperature	K/hr
CR chondrites							
	EET 92048	AO1	AO/PO	type II	OA3	673–873 K	0.6
	Gao-Guenie (b)	Ch1	PO	type II	A5	673–873 K[a]	0.3
	Gao-Guenie (b)	Ch2	BO/PO-comp	type II	A5	673–873 K[a]	1
	Gao-Guenie (b)	Ch12	POP	type II	A1	673–873 K[a]	4
	MIL 090657	Ch2	BO/PO	type II	OA2	673–873 K	0.6
	PCA 91082	Ch1	POP	type II	A3	673–873 K[a]	0.8
LL3.00 chondrite							
	Semarkona	Ch3	POP	type I	OA9	503–873K[b]	2
	Semarkona	Ch3	POP	type I	OA10	503–873K[b]	0.3

AO = agglomeratic olivine chondrule; Ch = chondrule; PO = porphyritic olivine; BO = barred olivine; POP = porphyritic olivine pyroxene; comp = compound; type II = FeO-rich; type I = FeO-poor.
OA = opaque assemblage; A = assemblage.
a. Sulfide equilibration temperature from Schrader et al. (2015).
b. Sulfide equilibration temperature from Schrader et al. (2016).

FIGURES

Figure 1

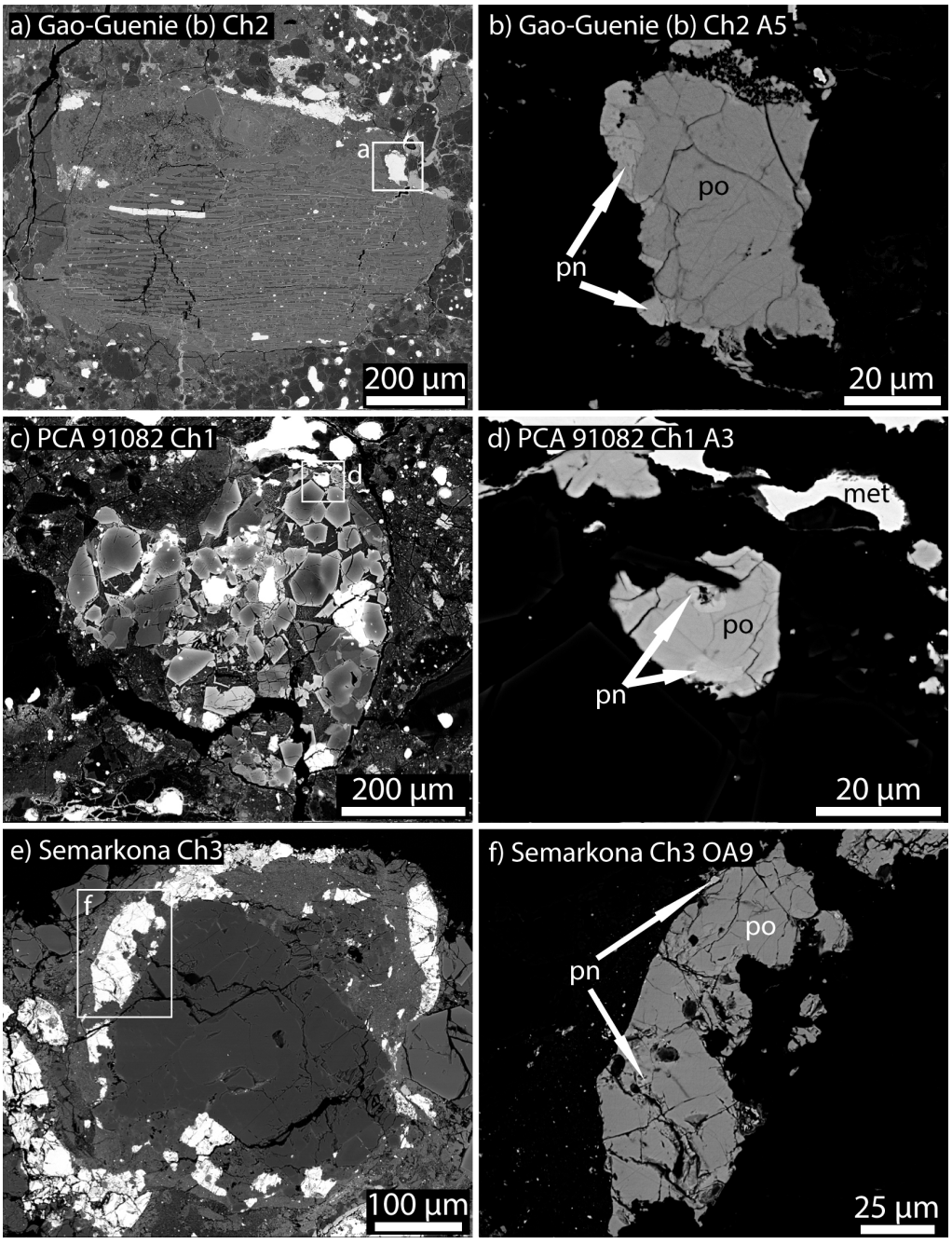

Fig. 1. Backscattered electron images of chondrules with sulfide assemblages containing pyrrhotite (po) with pentlandite (pn) in a,b) Gao-Guenie (b) (CR2), c,d) PCA 91082,15 (CR2), and e, f) Semarkona (LL3.00). a) Gao-Guenie (b) Ch2, a type II (FeO-rich) barred olivine

chondrule. b) Pyrrhotite-pentlandite assemblage in Gao-Guenie (b) Ch2. c) PCA 91082,15 Ch1, a type II porphyritic olivine pyroxene (POP) chondrule. d) Pyrrhotite-pentlandite assemblage in PCA 91082,15 Ch1. e) Semarkona Ch3, a type I (FeO-poor) POP chondrule. f) Pyrrhotite-pentlandite assemblage in Semarkona Ch3. Regions in black in b, d, and e are silicate minerals. Where: met = Fe,Ni metal.

Figure 2

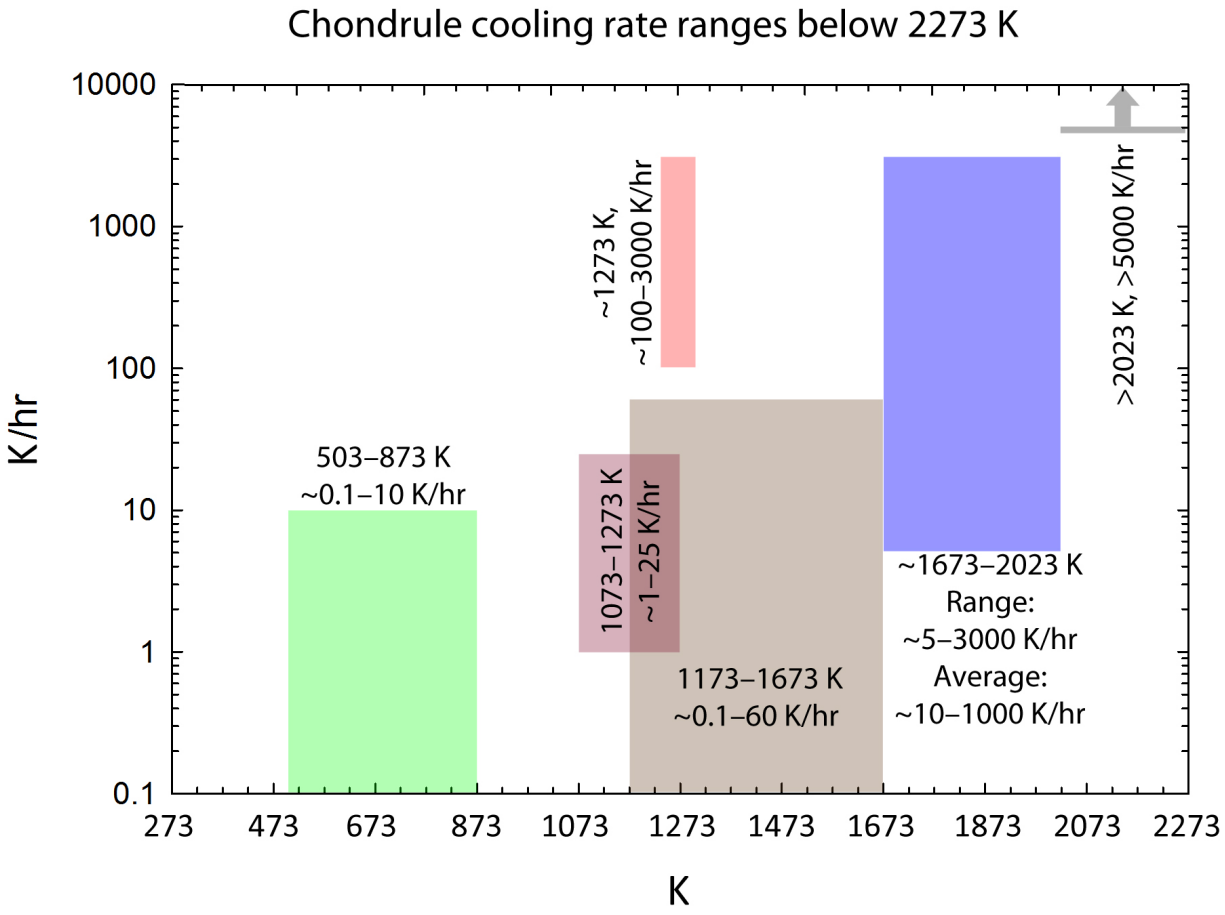

Fig. 2. Chondrule cooling rates, K vs. K/hr: > 2023 K from (Yu and Hewins, 1998); 1673–2023 K from (Radomsky and Hewins, 1990; Desch and Connolly, 2002; Hewins et al., 2005; Berlin et al., 2011; Desch et al., 2012); 1173–1673 K from (Weinbruch et al., 2001; Humayun, 2012; Chaumard et al., 2018); 1073–1273 K from (Wick and Jones, 2012); and ~1273 K from (Tachibana et al., 2006, Schrader and Lauretta, 2010). The cooling rate for 503–873 K is from this study.

ELECTRONIC ANNEXES

Electronic Annex-1 (mmc1): Backscattered electron images of sulfides and host chondrules.

Electronic Annex-2 (mmc2): In situ major and minor element compositions of sulfides obtained via electron microprobe analysis, in weight %.